EGU2020: Sharing Geoscience Online
04. May 2020, 16:15 – 18:00 CET

Comparison of Coupling Methods in Joint Inversion along the Namibian Continental Margin

(EGU2020-20720)

Gesa Franz[1], Max Moorkamp[2], Marion Jegen[1], Christian Berndt[1],Wolfgang Rabbel[3]

[1]GEOMAR Helmholtz Centre for Ocean Research Kiel
[2]Munich University, Department of Earth and Environmental Sciences, Geophysics
[3]Kiel University, Institute of Geosciences, Applied Geophysics

HELMHOLTZ
RESEARCH FOR GRAND CHALLENGES

GEOMAR

Introduction

Geophysical inversion always faces the problem of ambiguity, where several earth models can describe the same data.

To tackle this issue, additional information can be integrated by joint inversion of different data sets (Heincke et al., 2017; Moorkamp, 2017; Moorkamp et al., 2011), or by cooperative inversion through relating physical models derived from independent data (Bedrosian, 2007; Gallardo, 2004; Haber & Oldenburg, 1997; Lines et al., 1987; Paasche & Tronicke, 2007).

Here we present our recent results of joint- and cooperative inversions along the Namibian passive continental margin and Walvis Ridge investigating break-up related magmatism. Jegen et al. (2016), presents a resistivity model derived from Magnetotelluric data acquired in 2011 (SAMPLE project). We reevaluate this data due to a previous rotation error, and implement three additional set ups, where

a) MT data inversion is constrained by a geological model derived from gravity modeling (Maystrenko et al., 2013)

b) marine MT- and satellite gravity data are jointly inverted with a common objective function

c) a 2D velocity model (Fromm et al., 2017) is used as a structural constraint in 3D MT inversion

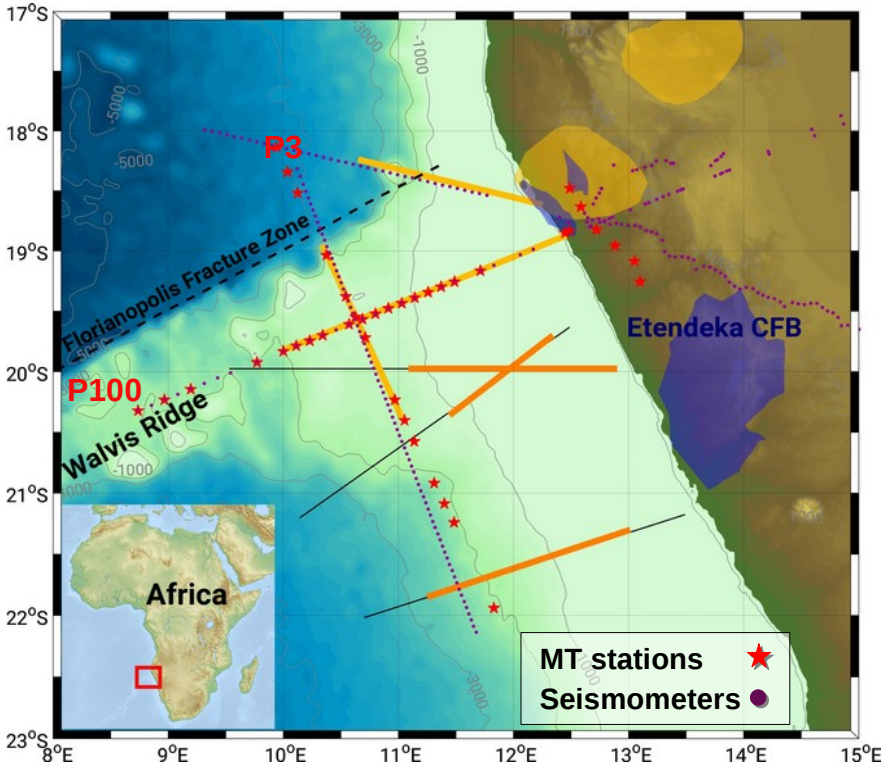

Interpretation of break-up related magmatic features in seismic studies:

magm. underplating (Fromm et al., 2015 and Planert et al., 2016)

magm. underplating (Gladczenko et al., 1998)

high v_p/v_s ratios (Heit et al., 2015)

a) MT data inversion constrained by a model derived from gravity modeling

Pseudosections of MT data:

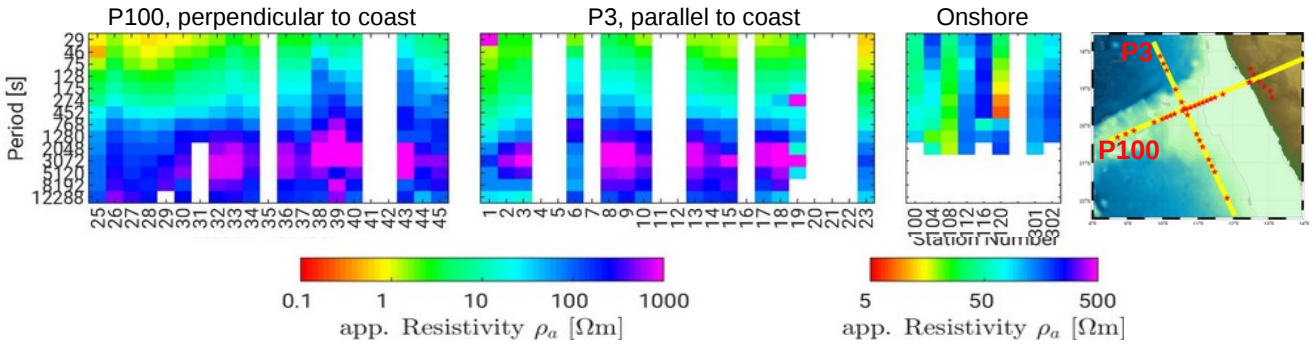

Geological model derived from gravity modeling (Maystrenko et al., 2013):

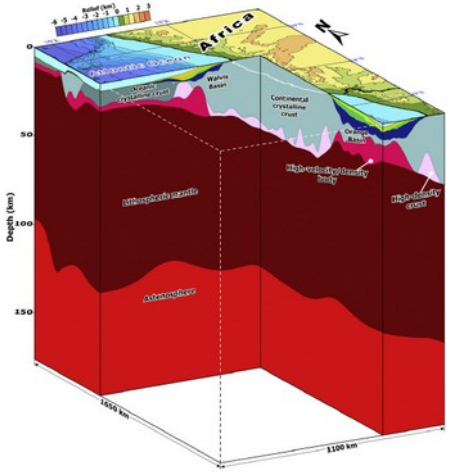

Objective function:

$$\Phi(m) = \Phi_{d_{MT}}(m) + \lambda_{MT}\Phi_{Reg_{MT}}(m) + \kappa\Phi_{Cross}(m)$$ with cross-gradient coupling term

$$\Phi_{Cross}(m) = (\nabla m_{res} \times \nabla m_{struct})^T C_M^{-1} (\nabla m_{res} \times \nabla m_{struct})$$

Moorkamp et al. (2011), Gallardo & Meju (2003)

The Magnetotelluric data was recorded on two research cruises (MSM17-1/2) at the turn of the years 2010/11, and during a land survey in Fall 2011 (Kapinos et al., 2016). Our inversion input consists of 32 marine and 8 land stationscovering frequencies from $2 \cdot 10^{-5}$ – 10^{-1} Hz. The pseudosections suggest high apparent resistivity at mid-crustal depths and a complex onshore structure.

3D joint and cooperative inversion is conducted using the framework jif3D (Moorkamp et al., 2011). The objective function includes the cross-gradient coupling term Φ_{cross}, which enforces structural similarity of the inversion model m_{res} to a given and unchanging cross model m_{Cross} by minimizing the cross product of their spatial gradients. The integrated cross model is the geological model of densities by Maystrenko et al. (2013). Their model consists of sediments, normal oceanic- and continental crust, high density oceanic- and continental crust, and a lithospheric mantle.

b) Joint inversion of marine MT and satellite gravity data

Pseudosections of MT data:

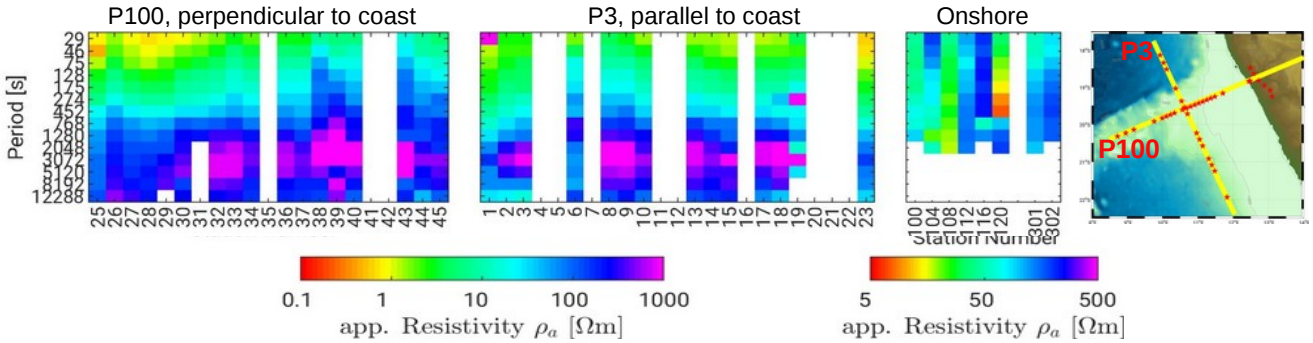

Satellite gravity data corrected for topography and crustal thickness:

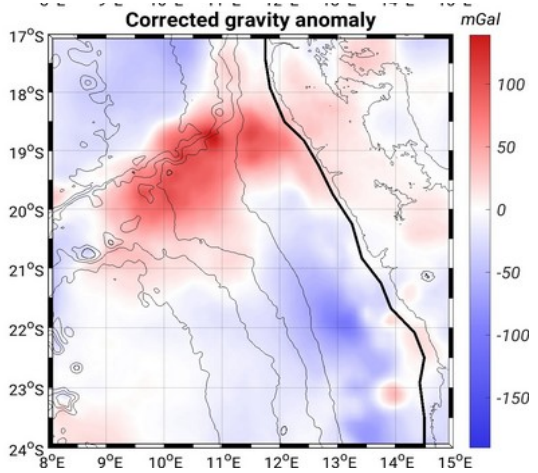

Objective function:

$$\Phi(m)=\Phi_{d_{MT}}(m)+\Phi_{d_{Grav}}(m)+\lambda_{MT}\Phi_{Reg_{MT}}(m)+\lambda_{Grav}\Phi_{Reg_{Grav}}(m)+\kappa\Phi_{Cross}(m)$$ with

Data misfit: $\Phi_d(m)=[g(m)-d_{obs}]^T C_d^{-1}[g(m)-d_{obs}]$

Regularization misfit: $\Phi_{Reg}(m)=\sum_i \alpha_i m^T W_i^T C_m^{-1} W_i m$ Moorkamp et al. (2011)

g(m) - model data | C_d - data covariance | α - directional weight | W - spatial derivatives of model parameters

d_{obs} - observed data | C_m - model covariance | i - Cartesian direction i={x,y,z}

For the second integrated approach, we combine the MT data with satellite gravity data. The EIGEN-6C4 anomaly data (Barthelmes & Köhler, 2016; Ince et al., 2019) is corrected for topography/bathymetry and crustal thickness to account for the drastic change at the coast. This corrected data shows a strong positive anomaly at the landfall of Walvis Ridge, suggesting increased densities.

Gravity data- and regularization terms ($\Phi_{d,Grav}$ and $\Phi_{reg,Grav}$, respectively) are added to the objective function as shown above. The cross-gradient is now calculated for the two changing models m_{res} and m_{dens}.

c) MT data inversion constrained with a 2D velocity model

Pseudosections of MT data:

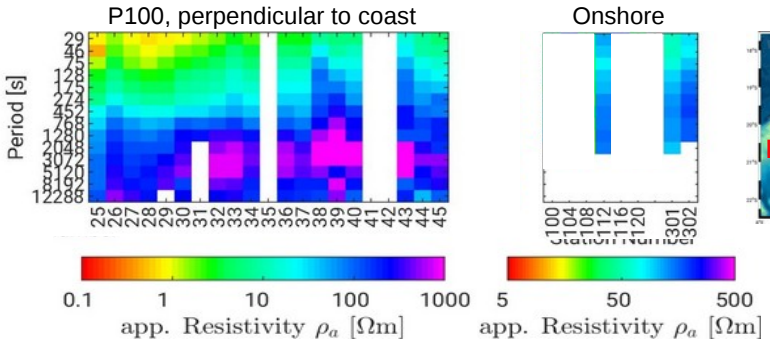

2D seismic model along P100 derived from seismic modeling (Fromm et al., 2017):

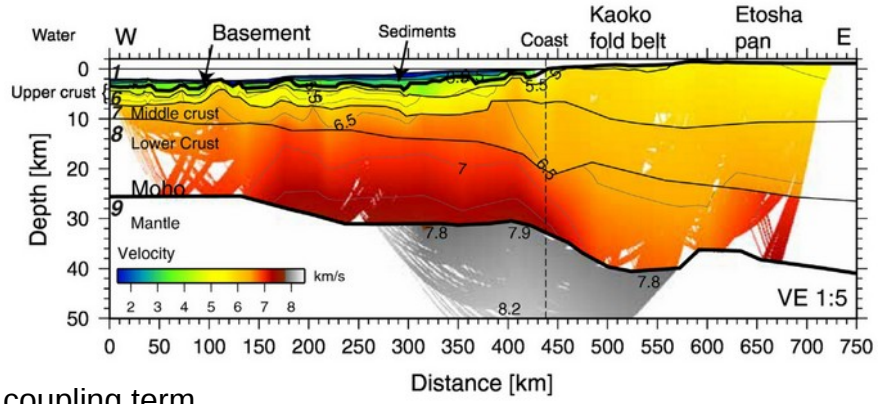

Objective function:

$$\Phi(m) = \Phi_{d_{MT}}(m) + \lambda_{MT}\Phi_{Reg_{MT}}(m) + \kappa\Phi_{Cross}(m)$$

with cross-gradient coupling term

$$\Phi_{Cross}(m) = (\nabla m_{res} \times \nabla m_{vel})^T C_M^{-1} (\nabla m_{res} \times \nabla m_{vel})$$

Moorkamp et al. (2011), Gallardo & Meju (2003)

For the third coupling approach, we want to include the 2D velocity model along profile 100 by Fromm et al. (2017) with the MT data inversion. To account for the complex topography in the study area, we chose to 3D invert the MT data for a narrow cube around the profile (50 km to each side) and consider this “quasi-2D” for the cross-gradient coupling.

Due to the nature of cross-gradient coupling constraint, which is zero wherever one of the two models is zero, we suspect, that approach a) of coupling MT inversion with a structural model, may not have a strong influence, because the cross model has large blocks of a constant parameter. Therefore, it only enforces a structural constraint on its formation’s boundaries. For this reason, we wanted to test whether a smooth cross model has a stronger impact, and selected this velocity model derived from data of the same project/cruise. Tests on the influence of the “quasi-2D” approach here concluded, that the narrow model leads to a slight loss of 3D information, but fits were acceptable (RMS of 2.81 compared to 2.37 with a whole 3D model) .

Data fits (Pseudosections)

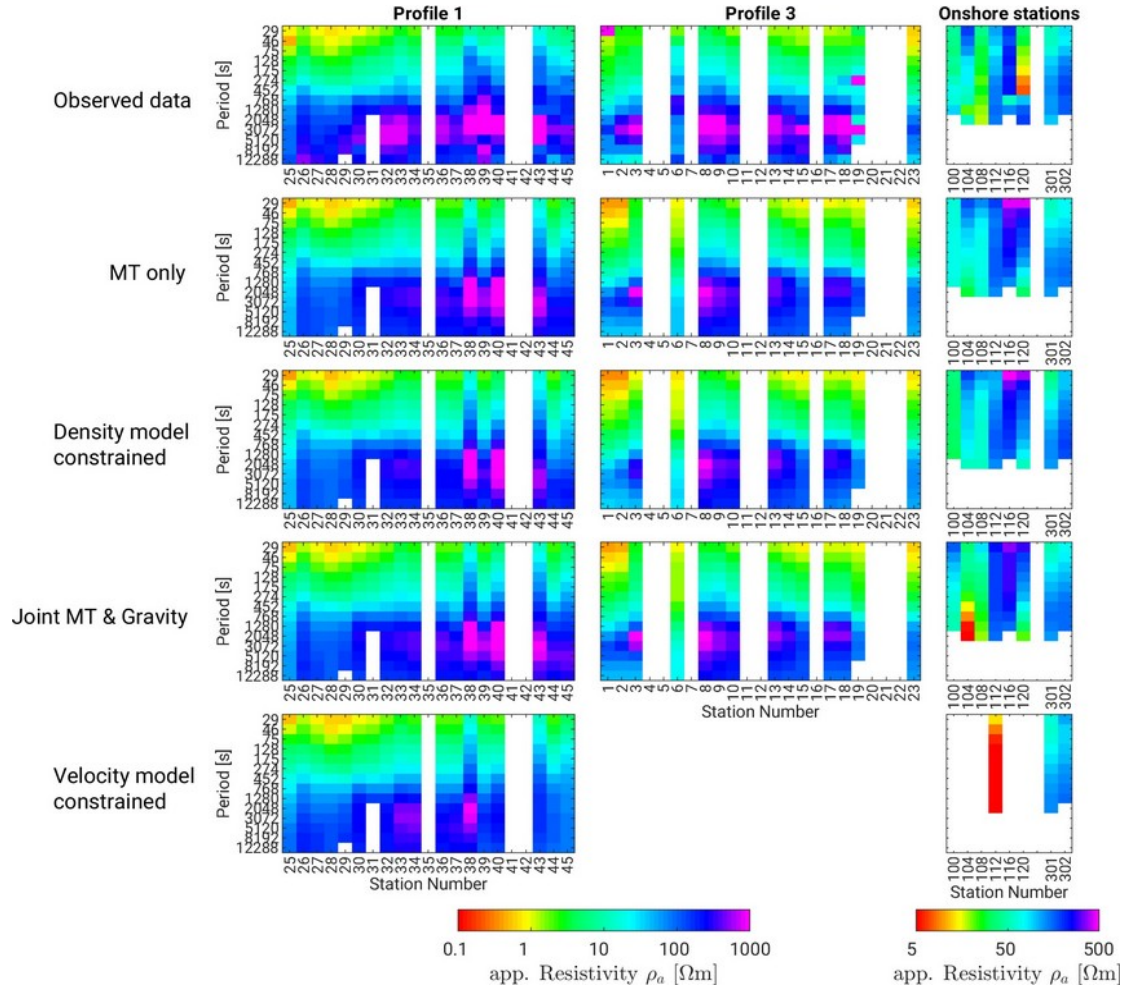

- **observed data** show low apparent resistivites in shorter periods
  - ➔ indicate variation in sediment thickness
- **observed data** show high apparent resistivities at intermediate periods
  - ➔ indicate highly resistive magmatic underplating
- **observed onshore data** has large variations in neighboring stations
  - ➔ indicate complex resistivity structure

- in all **inversion model's data** (lower 4 pseudosections): low app. resistivities at low periods & high app. resistivities at intermediate periods are well represented
- **however**: highest resistivity values don't reach maximum values of observed data
  - ➔ e.g. st. 30-33 & 15-18: inversion model's data have at most slightly increased app. resistivity, while observed data show clear peaks
- strong **onshore** variations are not fitted well during inversion

Model comparison along profiles

P100, perpendicular to coast

P3, parallel to coast

Black lines are velocity contours of 2D model by Fromm et al. (2017)

Black lines are velocity contours of 2D model by Planert et al. (2016)

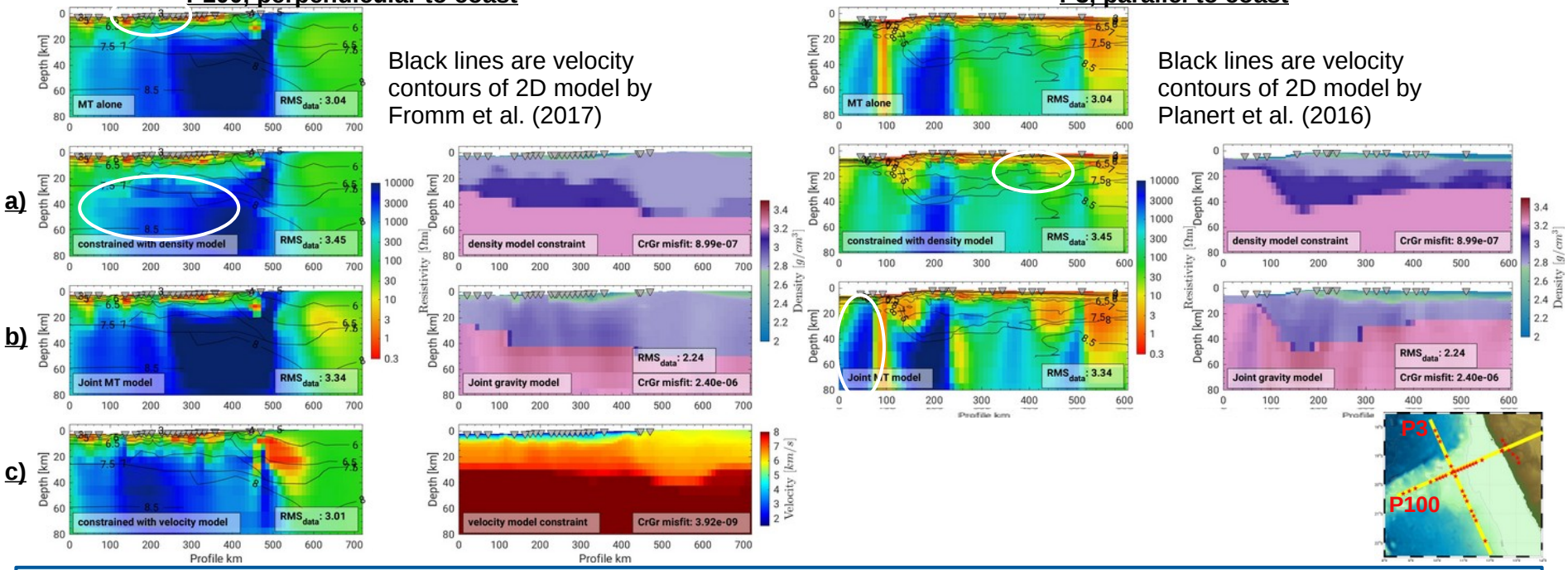

Key differences we aim to discuss:

- **shallow conductors** → decreased resistivity concurs with sedimentary basins along Walvis Ridge (Goslin et al., 1974) and at the ridge's landfall (Fromm et al., 2017), the southern conductive anomalies concur with findings of seaward dipping reflectors (Gladczenko et al, 1998; Elliot et al., 2009) as imaging of inter layered basaltic flows
- **high resistivity body** at middle-lower crustal depths → lateral concordance with observed magmatic underplating (Fromm et al., 2017; Planert et al., 2016; Gladczenko et al., 1998; Maystrenko et al., 2013)
- **vertical, deep conductor** along P3 at 90 km → possibly matching Florianopolis fracture zone north of Walvis Ridge, which has been imaged as an abrupt change in crustal thickness (Planert et al., 2016, Sibuet et al., 1984, Goslin et al., 1975)

Model comparison, 3D features

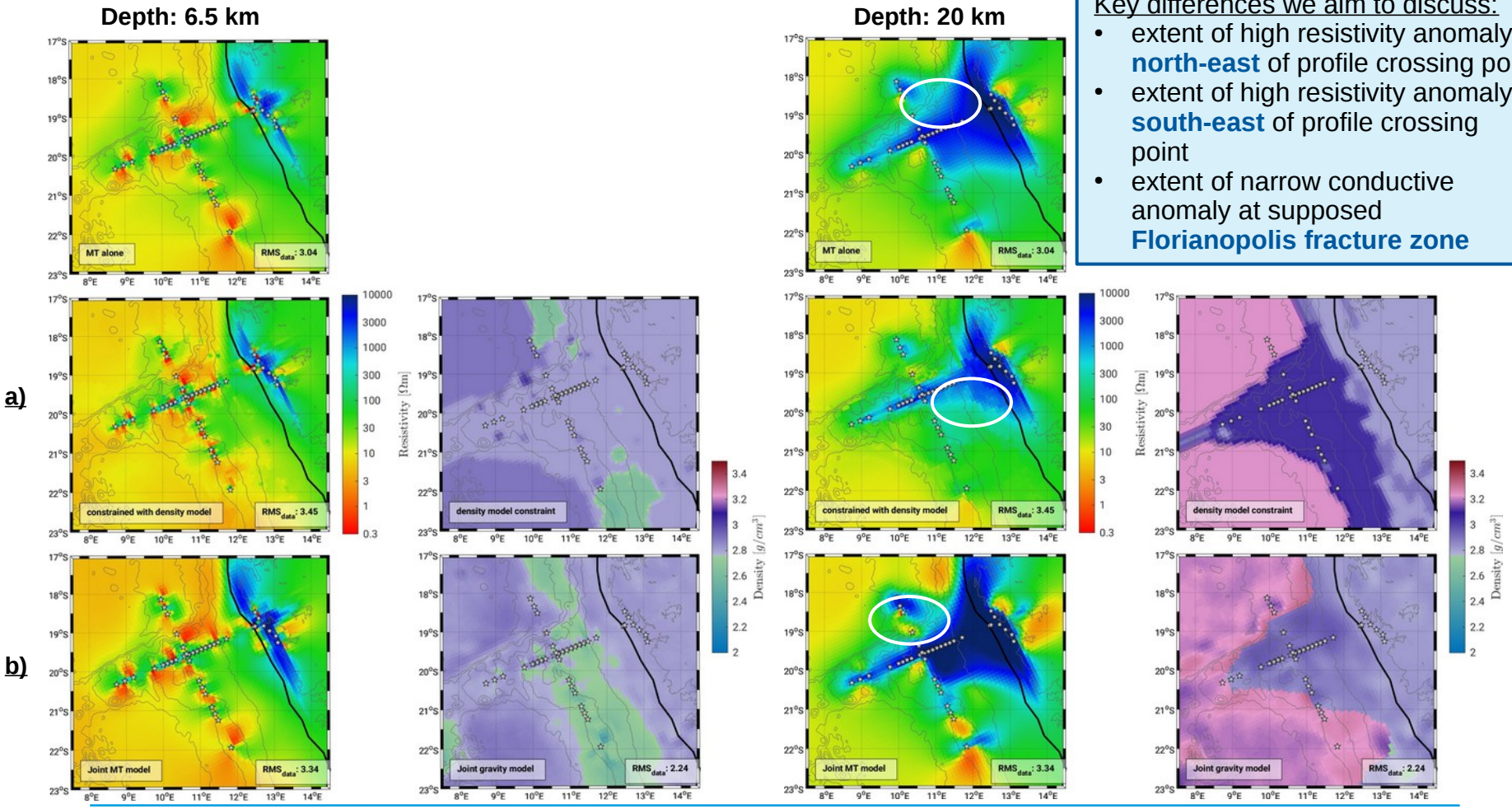

Key differences we aim to discuss:

- extent of high resistivity anomaly **north-east** of profile crossing point
- extent of high resistivity anomaly **south-east** of profile crossing point
- extent of narrow conductive anomaly at supposed **Florianopolis fracture zone**

Model comparison along profiles

- **shallow conductors ⇔ sediment thickness**
  - MT only: thickness ~6-10 km, internally smooth
  - a) Structural model constrained: thickness ~8-15 km, internal boundaries visible at ~2-4 km thickness
  - b) Joint inversion: thickness ~8-15 km, internally smooth
  - c) Gradient model constrained: thickness ~6-8 km, internally smooth
  - **References*: thickness ~2-6 km**

- **high resistivity body ⇔ magmatic underplating**
  - MT only: highest resistivity between profile crossing and landfall, from ~30 km downwards, anomaly continues south-east of profile crossing, internally smooth
  - a) Structural model constrained: highest resistivity close to landfall, from ~40 km downwards, anomaly limited to beneath MT stations, internal boundaries visible at supposed Moho depth of cross model
  - b) Joint inversion: highest resistivity between profile crossing and landfall, from ~20 km downwards, anomaly continues strongly south-east of profile crossing, internally smooth
  - c) Gradient model constrained: highest resistivity close to profile crossing, from ~30 km downwards, internally smooth
  - **References*: thick, high velocity/density crust beneath Walvis Ridge, from ~20 km down, thickness ~8-30 km**

- **vertical, deep conductor ⇔ Florianopolis fracture zone**
  - MT only: conductor ~30 km wide, 100 km deep
  - a) Structural model constrained: no conductor visible
  - b) Joint inversion: conductor ~40-60 km wide, 200+ km deep (entire model)
  - c) Gradient model constrained: *-not covered by model-*
  - **References*: abrupt decrease in crustal thickness**

***References**:
Fromm et al. (2017)
Gladczenko et al. (1998)
Goslin et al. (1974)
Goslin et al. (1975)
Maystrenko et al. (2013)
Planert et al. (2016)
Sibuet et al. (1984)

Tests to estimate resolution capabilities

We conduct tests to investigate whether these model differences and discrepancies are within the resolution capabilities of our inversion set up. For these tests, we manually modify the inversion model, calculate a forward response and compare data fits, and response curves. We focus discussion on the three aforementioned model features:

- **shallow conductors ⇔ sediment thickness**
  - simultaneous decrease of anomaly thickness and resistivity does not corrupt data fit (MT method is mostly sensitivity for conductance (conductivity-thickness-product))
    - ➔ Sediments could also be thinner and more conductive

- **high resistivity body ⇔ magmatic underplating**
  - reducing thickness of anomaly (even when increasing resistivity) results in corruption of data fit
  - removing anomalies north-east and south-east of profile crossing does not corrupt data fit, as long as model is consistent directly next to MT stations
    - ➔ resistivity anomaly needs to be deep (>100 km)
    - ➔ statement about extent away from profiles is unreliable

- **narrow, deep conductor ⇔ Florianopolis fracture zone**
  - low resistivity values are needed to fit data
  - simultaneous drastic decrease in extent, and slight decrease in resistivity does not corrupt data fit
  - resolution for lateral extension of anomaly along supposed fracture zone (north of Ridge) is not given
    - ➔ anomaly could be distinctively shallower (10-15 km), and a linear feature following the Florianopolis fracture zone

Summary of observations

MT inversion coupled with structural model:

- internal boundaries in shallow conductors indicate thinner sediments (in accordance with reference observations, feasible according to tests)
- internal boundary in mid-crustal resistor indicates resistivity change at Moho (in accordance with reference observations, thinner resistor is not feasible according to tests)
- suppression of deep conductor at 90 km on P3 (anomaly is distinctively shallower, in accordance with reference observations of a crustal fracture zone, feasible according to tests)

Joint inversion of MT and gravity data:

- shallow conductors indicate thicker sediments (contradicts reference observations)
- mid-crustal high resistivity anomaly sits shallower (in accordance with reference observations)
- stronger & deeper conductor at 90 km on P3 (contradicts reference observations)

MT inversion coupled with gradient model in “quasi-2D” approach:

- shallow conductors indicate thicker sediments (contradicts reference observations)
- mid-crustal high resistivity anomaly is further offshore, while onshore resistivities are strongly reduced (hints at alternative way of fitting of coast effect)

Conclusions

MT inversion with a cross-gradient coupled model constraint	Joint inversion of MT and gravity data
++ helps eliminating excessive smearing • significantly smaller depth extent of fracture zone anomaly • high resistivities northeast and southeast of profile crossing • shallower sediments • gives an alternative option to fit electromagnetic coast effect	++ possible improvement of density model • here we question improvement, because the density model changes are mainly focused on the 'doubtful' features
+− weakening/suppression of features • mid-crustal resistor less prominent (here it reduces data fit, but in other setups, this could be beneficial)	+− features of resistivity model are enhanced • mid-crustal resistor has higher resistivity and sits shallower • Deeper conductor at fracture zone
−− introduces patchiness in resistivity model at constrained model boundaries	−− density anomalies are smeared • The features we question in the resistivity model are traced to the density model

References

Thank you for your interest – session chat is on Monday, May 4th, 4:15 – 6 P.M.

References:

Barthelmes, F., & Köhler, W. (2016). International Centre for Global Earth Models (ICGEM). In *The Geodesists Handbook 2016* (pp. 907–1205). https://doi.org/10.1007/s00190-016-0948-z

Bedrosian, P. A. (2007). MT+, integrating magnetotellurics to determine earth structure, physical state, and processes. *Surveys in Geophysics*, *28*(2–3), 121–167. https://doi.org/10.1007/s10712-007-9019-6

Elliott, G. M., Berndt, C., & Parson, L. M. (2009). The SW African volcanic rifted margin and the initiation of the Walvis Ridge, South Atlantic. *Marine Geophysical Researches*, *30*(3), 207–214. https://doi.org/10.1007/s11001-009-9077-x

Fromm, T., Jokat, W., Ryberg, T., Behrmann, J. H., Haberland, C., & Weber, M. (2017). The onset of Walvis Ridge: Plume influence at the continental margin. *Tectonophysics*.

Gallardo, L. A. (2004). Joint two-dimensional DC resistivity and seismic travel time inversion with cross-gradients constraints. *Journal of Geophysical Research*, *109*(B3), n/a–n/a. https://doi.org/10.1029/2003jb002716

Gallardo, L. A., & Meju, M. A. (2003). Characterization of heterogeneous near-surface materials by joint 2D inversion of dc resistivity and seismic data. *Geophysical Research Letters*, *30*(13). https://doi.org/10.1029/2003GL017370

Gladczenko, T. P., Skogseid, J., & Eldhom, O. (1998). Namibia volcanic margin. *Marine Geophysical Research*, *20*(4), 313–341. https://doi.org/10.1023/A:1004746101320

Goslin, J., Mascle, J., Sibuet, J.-C., & Hoskins, H. (1974). Geophysical study of the easternmost Walvis Ridge, South Atlantic: Morphology and shallow structure. *Geological Society of America Bulletin*, *85*(4), 619–632. https://doi.org/10.1130/0016-7606(1974)85<619:GSOTEW>2.0.CO;2

Goslin, J., & Sibuet, J. C. (1975). Geophysical study of the easternmost Walvis Ridge, South Atlantic: Deep structure. *Bulletin of the Geological Society of America*, *86*(12), 1713–1724. https://doi.org/10.1130/0016-7606(1975)86<1713:GSOTEW>2.0.CO;2

Haber, E., & Oldenburg, D. (1997). Joint inversion: A structural approach. *Inverse Problems*, *13*(1), 63–77. https://doi.org/10.1088/0266-5611/13/1/006

Heincke, B., Jegen, M., Moorkamp, M., Hobbs, R. W., & Chen, J. (2017). An adaptive coupling strategy for joint inversions that use petrophysical information as constraints. *Journal of Applied Geophysics*, *136*, 279–297. https://doi.org/10.1016/j.jappgeo.2016.10.028

Heit, B., Yuan, X., Weber, M., Geissler, W., Jokat, W., Lushetile, B., & Hoffmann, K.-H. (2015). Crustal thickness and Vp/Vs ratio in NW Namibia from receiver functions: Evidence for magmatic underplating due to mantle plume-crust interaction. *Geophysical Research Letters*, *42*(9), 3330–3337. https://doi.org/10.1002/2015GL063704

Ince, E. S., Barthelmes, F., Reißland, S., Elger, K., Förste, C., Flechtner, F., & Schuh, H. (2019). ICGEM – 15 years of successful collection and distribution of global gravitational models, associated services, and future plans. *Earth System Science Data*, *11*(2), 647–674. https://doi.org/10.5194/essd-11-647-2019

Jegen, M., Avdeeva, A., Berndt, C., Franz, G., Heincke, B., Hölz, S., Neska, A., Marti, A., Planert, L., Kopp, H., Baba, K., Ritter, O., Weckmann, U., Meqbel, N., & Behrmann, J. (2016). 3-D magnetotelluric image of offshore magmatism at the Walvis Ridge and rift basin. *Tectonophysics*, *683*, 98–108. https://doi.org/10.1016/j.tecto.2016.06.016

Kapinos, G., Weckmann, U., Jegen-Kulcsar, M., Meqbel, N., Neska, A., Katjiuongua, T. T., Hölz, S., & Ritter, O. (2016). Electrical resistivity image of the South Atlantic continental margin derived from onshore and offshore magnetotelluric data. *Geophysical Research Letters*, *43*(1), 154–160.

Lines, L., Schultz, A. K., & Treitel, S. (1987). Cooperative inversion of geophysical data. *1987 SEG Annual Meeting*, *53*(1), 814–816. https://doi.org/10.1306/703c8d7b-1707-11d7-8645000102c1865d

Maystrenko, Y. P., Scheck-Wenderoth, M., Hartwig, A., Anka, Z., Watts, A. B., Hirsch, K. K., & Fishwick, S. (2013). Structural features of the Southwest African continental margin according to results of lithosphere-scale 3D gravity and thermal modelling. *Tectonophysics*, *604*, 104–121. https://doi.org/10.1016/j.tecto.2013.04.014

Moorkamp, M. (2017). Integrating Electromagnetic Data with Other Geophysical Observations for Enhanced Imaging of the Earth: A Tutorial and Review. *Surveys in Geophysics*, *38*(5), 935–962. https://doi.org/10.1007/s10712-017-9413-7

Moorkamp, M., Heincke, B., Jegen, M., Roberts, A. W., & Hobbs, R. W. (2011). A framework for 3-D joint inversion of MT, gravity and seismic refraction data. *Geophysical Journal International*, *184*(1), 477–493. https://doi.org/10.1111/j.1365-246X.2010.04856.x

Paasche, H., & Tronicke, J. (2007). Cooperative inversion of 2D geophysical data sets: A zonal approach based on fuzzy c-means cluster analysis. *Geophysics*, *72*(3), 35–39. https://doi.org/10.1190/1.2670341

Planert, L., Behrmann, J., Jokat, W., Fromm, T., Ryberg, T., Weber, M., & Haberland, C. (2016). The wide-angle seismic image of a complex rifted margin, offshore North Namibia: Implications for the tectonics of continental breakup. *Tectonophysics*.

Sibuet, J.-C., Hay, W. W., Prunier, A., Montadert, L., Hinz, K., & Fritsch, J. (1984). Early evolution of the South Atlantic Ocean: role of the rifting episode. *Initial Reports of the Deep Sea Drilling Project*, *75*, 469–481.

Addition: Apparent resistivity and phase of stations 2, 3, and 6